



Title	Internal-friction mapping on solids by resonance ultrasound microscopy
Author(s)	Ogi, H. ; Niho, H. ; Hirao, M.
Citation	Applied Physics Letters. 2006, 88(14), p. 141110-1-141110-3
Version Type	VoR
URL	https://hdl.handle.net/11094/84207
rights	This article may be downloaded for personal use only. Any other use requires prior permission of the author and AIP Publishing. This article appeared in Applied Physics Letters, 88(14), 141110 (2006) and may be found at https://doi.org/10.1063/1.2194479 .
Note	

The University of Osaka Institutional Knowledge Archive : OUKA

<https://ir.library.osaka-u.ac.jp/>

The University of Osaka

Internal-friction mapping on solids by resonance ultrasound microscopy

H. Ogi,^{a)} H. Niho, and M. Hirao

Graduate School of Engineering Science, Osaka University, Toyonaka, Osaka 560-8531, Japan

(Received 17 January 2006; accepted 26 February 2006; published online 6 April 2006)

An internal-friction microscopy is developed for quantitatively determining material damping on a local surface area by measuring vibrational attenuation of an isolated langasite oscillator point contacting the material. Noncontacting measurement of the resonance frequency and attenuation coefficient of the longitudinal vibration of the oscillator has been achieved with a line antenna, providing high sensitivity to the modulus and damping in the local contacting area. Formulation of the relationship between a material's local internal friction and attenuation of the resonator system is proposed using the generalized Hertzian-contact model. Results on a dual-phase stainless steel and a Cu/NbTi composite are shown. © 2006 American Institute of Physics.

[DOI: 10.1063/1.2194479]

A material's internal friction reflects mechanical losses caused by anelastic movements of dislocations, thermally activated diffusion of point defects, interactions between magnetic domains and mechanical vibrations, and so on, as explained in detail in monographs.^{1–3} In particular, internal friction shows high sensitivity to dislocations as proved by its continuous measurement during fatigue tests of metallic materials.^{4,5} The drastic change of the dislocation structure occurs only in a small surface area during fatigue, and internal friction should be measured locally. Measurement of internal friction in local areas is important in view of nondestructive evaluation as well as in the materials science field.

We recently developed a microscopy for determining the local modulus of materials using an isolated oscillator, which we call resonance ultrasound microscopy (RUM) (Refs. 6–8). Mechanical resonance frequencies of the oscillator change when it is in contact with a material, depending on the elastic constants of the material at the contact point. The oscillator's resonance-frequency shift then provides the material's local stiffness.

The oscillator's attenuation is also expected to evaluate the local damping of materials. However, the quantitative determination needs an isolated oscillator, because the Q value of the resonator system depends on all the mechanical contacts on the oscillator. We must prohibit other contacts other than the one with the measuring material. No study has achieved the quantitative evaluation of local damping because of unfavorable contacts. Therefore, we here intend to establish the RUM method to evaluate the local internal friction of solids and formulate the relationship between attenuation of the resonator system and the material's internal friction.

Figure 1(a) shows the setup of our home-built microscopy developed here. A rectangular-paralleliped monocrystal-langasite oscillator touches a specimen through a monocrystal diamond tip of 12 μm diam. The oscillator measures 6, 0.68, and 0.68 mm along the X , Y , and Z directions of trigonal crystallographic axes, respectively. We hold it by a fixture at the nodal line of the vibration so as to give little influence on the vibration from holding. The fixture and oscillator are placed in a cylindrical guide, which allows

only the vertical movement of the oscillator. Gravity applies a constant biasing force for contact. A line antenna is embedded in the guide to generate quasistatic electric field near the center line of the side face of the crystal, where the maximum stress occurs for an intended resonance. It consists of three straight wires, two for generation and detection, and the other for grounding. When a sinusoidal voltage is applied to the generation wire, the quasistatic electric field E_x occurs in the vertical direction, causing the principal stresses $-e_{11}E_x$ in the X direction and $e_{11}E_x$ in the Y direction via the converse piezoelectric effect. e_{11} denotes a piezoelectric coefficient of materials showing 32-point-group symmetry. Thus, this electric field causes the breathing vibrations (A_g vibration groups^{9,10}). After the excitation, the detection wire picks up the resonance vibration through the piezoelectric effect. A frequency scan yields the resonance spectrum contactlessly and the Lorentzian-function fitting provides the resonance frequency.¹¹ The resonance-frequency measurement is followed by the attenuation measurement: The amplitude decay with time is recorded after an excitation with the measured resonance frequency and the exponential-function fitting yields the attenuation coefficient α of the resonator system.¹¹

The specimen is put on the XYZ stage to scan the specimen surface measuring the resonance frequency and attenuation coefficient. All the components are placed in a vacuum (~ 1 Pa) to avoid acoustic noise and energy loss into air.

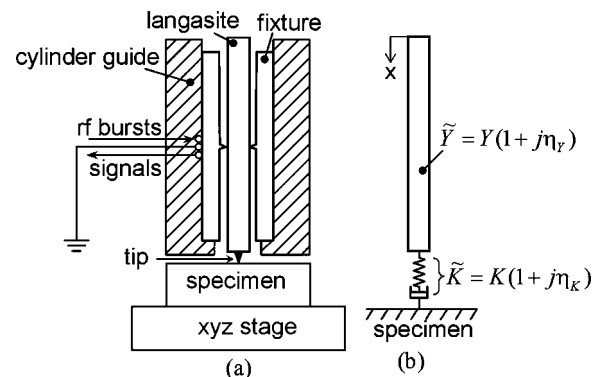


FIG. 1. (a) Setup of resonance ultrasound microscopy consisting of monocrystal-langasite oscillator, diamond tip, straight-line antenna, and an XYZ stage on which the specimen is placed. (b) A spring-dashpot model for analyzing the effective modulus and internal friction of the specimen.

^{a)}Electronic mail: ogi@me.es.osaka-u.ac.jp

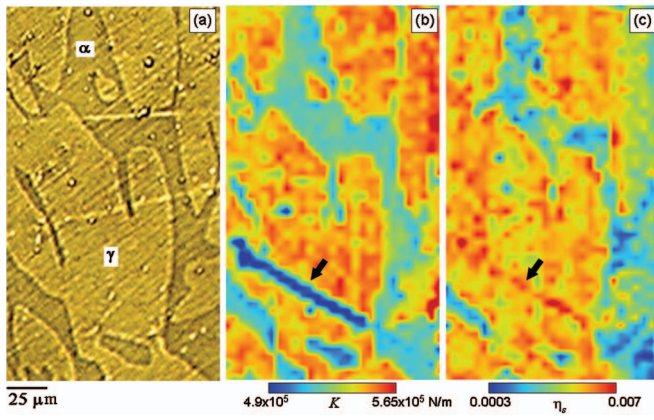


FIG. 2. (Color) (a) Optical-microscopy image, (b) contact-stiffness (K) image, and (c) internal-friction (η_e) image of a dual-phase stainless steel. Values for the stiffness and internal friction are given by the color bars. Measurements were done every $3 \mu\text{m}$ with a biasing force of 5.2 mN .

Langasite shows low-temperature derivatives of the elastic constants, of the order of 10^{-6} – 10^{-5} per Kelvin, requiring no temperature controlling.

We used the fundamental mode of the breathing resonance (A_g-1) because it has nodal lines of deformation at the center on the side faces and an antinode point at the center on the bottom surface, where the tip is attached to contact the specimen.

We approximate the A_g-1 vibration with the fundamental bar-resonance vibration and formulate the relationship between the observable system's attenuation α and the material's internal friction. This approximation is reasonable because the aspect ratio of the oscillator is large enough. (The difference between the resonance frequency of the three-dimensional A_g-1 mode and that calculated with the simple bar-resonance formula was less than 1% in the present case.) Figure 1(b) shows the model for the resonator system. Such a simple model can be applied only for the resonator system with an isolated oscillator. We consider that the contact at the tip-specimen interface is equivalent to the complex contact stiffness $\tilde{K} = K(1 + j\eta_K)$. K and η_K denote the stiffness and loss at the contact interface. The governing equation is

$$\rho \frac{\partial^2 u}{\partial t^2} = \tilde{Y} \frac{\partial^2 u}{\partial x^2}. \quad (1)$$

Here, u denotes the longitudinal displacement, $\tilde{Y} = Y(1 + j\eta_Y)$ is the complex Young's modulus in the X axis of the oscillator, and ρ denotes the mass density of the oscillator. The uniaxial coordinate x is taken downward from the top surface of the oscillator. Boundary conditions are

$$\tilde{Y} \frac{\partial u}{\partial x} = 0 \text{ at } x = 0 \text{ and } \tilde{Y} A \frac{\partial u}{\partial x} + \tilde{K} u = 0 \text{ at } x = L, \quad (2)$$

where L and A denote the length and cross-section area of the oscillator, respectively. These equations yield the general solution as $u = \text{const}(e^{j(\tilde{\omega}t - \tilde{\beta}x)} + e^{j(\tilde{\omega}t + \tilde{\beta}x)})$. Here, $\tilde{\omega} = \omega(1 + j\eta_\omega)$ is the complex angular frequency and η_ω equals attenuation of the system that is given by $\alpha/2\pi f$ with the attenuation coefficient α and resonance frequency f of the system. $\tilde{\beta} = \beta(1 + j\eta_\beta)$ denotes the wave number satisfying relation-

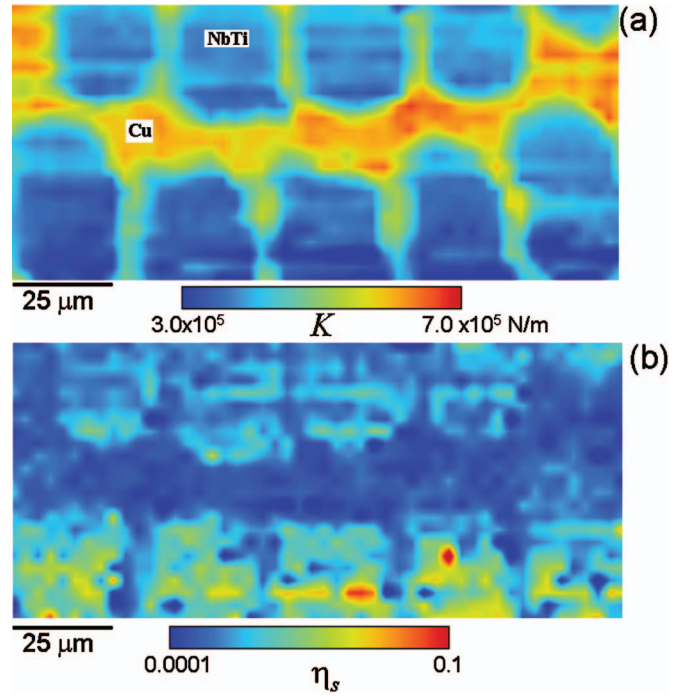


FIG. 3. (Color) (a) The stiffness and (b) internal friction images of a Cu/NbTi superconducting-wire composite. Measurements were done every $3 \mu\text{m}$ with a biasing force of 5.2 mN .

ships $\beta = \omega\sqrt{\rho/Y}$ and $\eta_\beta = \eta_\omega - \eta_Y/2$. Assuming $\eta_Y \ll 1$ and $\eta_K \ll 1$, we obtain

$$\beta L \tan(\beta L) = \frac{K}{K_{osc}} \equiv p, \quad (3)$$

$$\eta_\omega = \frac{\eta_Y(\beta L)^2 - p}{2(\beta L)^2 + p} + \frac{p}{(\beta L)^2 + p} \eta_K + \eta_{prop}, \quad (4)$$

where $K_{osc} = YA/L$ is the spring constant of the oscillator for a static load. p represents the contribution of the contact stiffness to the resonator system; larger p implies higher sensitivity to the modulus and damping of the specimen. (We selected the X axis of the langasite crystal to be vertical because the X -direction Young's modulus is the smallest to provide a larger p value.) Usually, $p \ll (\beta L)^2$ is satisfied and assumed to derive Eqs. (3) and (4). We added η_{prop} in Eq. (4), the background energy loss due to the sound propagation into the stage through the specimen, which is unavoidable in all contact measurements. This value is, however, estimated by measuring η_ω for the contact with very low-damping monocrystal silicon ($\eta_K \approx 0$). In the present case, it was of the order of 10^{-5} and much smaller than the system's damping.

Equations (3) and (4) give the resonance frequency and the damping value of the system, respectively. Note that they reduce to $\beta L = \pi$ and $\eta_\omega = \eta_Y/2$ when $p = 0$, confirming solutions for the free vibration without any contact.

According to the Hertzian-contact theory,¹² the contact stiffness is given by the material's stiffness as $K = \sqrt[3]{6FRY_{eff}^2}$. We assume that this relationship holds for the complex stiffnesses including damping factors

$$\tilde{K} = \sqrt[3]{6FR\tilde{Y}_{eff}^2} \quad (5)$$

Here, F and R denote the biasing force and tip radius, respectively. \tilde{Y}_{eff} is the effective stiffness of the material given by

$$\tilde{Y}_{eff} = [(1 - \nu_{tip}^2)/\tilde{Y}_{tip} + (1 - \nu_s^2)/\tilde{Y}_s]^{-1}, \quad (6)$$

where ν denotes Poisson's ratio. Subscripts *tip* and *s* indicate quantities of the diamond tip and the specimen, respectively. The losses accompanied by Poisson's ratios were omitted because of their negligible contributions to the system's damping. We use the polycrystal values of Young's modulus and Poisson's ratio for the diamond tip because of three reasons. (i) Its crystallographic orientation is unknown. (ii) The diamond's Young's modulus is much larger than the specimen's moduli and has little effect on the stiffness given by Eq. (6). (iii) Diamond shows a low anisotropic factor, and Young's modulus does not show strong dependence on the direction.

The material's internal friction η_s indicates the imaginary part of the complex modulus [$\tilde{Y}_s = Y_s(1 + j\eta_s)$] and it is related with η_K via

$$\eta_s = \frac{3}{2} \left[1 + \frac{Y_s}{Y_{tip}} \frac{1 - \nu_{tip}^2}{1 - \nu_s^2} \right] \eta_K - \frac{Y_s}{Y_{tip}} \frac{1 - \nu_{tip}^2}{1 - \nu_s^2} \eta_{tip}. \quad (7)$$

Thus, measuring the frequency and attenuation of the system at a local point, we can evaluate the material's stiffness K and damping η_s from Eqs. (3)–(7) simultaneously.

Figures 2(a)–2(c) compare images obtained by optical microscopy and RUM on a dual-phase stainless steel (JIS SCS-14A). It consists of a ferritic-phase (α -phase) matrix and austenitic-phase (γ -phase) precipitates.¹³ The volume fraction of the α phase is 25.8%. (We assumed $\nu_s = 0.3$ and $\eta_{tip} = 10^{-5}$.) The RUM images clearly show the difference of the elastic and damping properties between the two phases. The specimen surface was simply mechanical polished using emery papers; RUM measurements show tolerance for the surface condition. Stiffness of the γ phase is principally higher than that of the α phase, which is attributed to the lower chromium concentration in the f.c.c. phase. Internal friction of the γ phase is larger than that of the α phase, indicating higher dislocation damping because of lower Peierls stress in the f.c.c. phase.¹⁴ The arrows in Figs. 2(b) and 2(c) may indicate a twin in the γ -phase grain, which is not observed by the optical microscopy.

Figures 3(a) and 3(b) show the stiffness and internal-friction images of a composite composed of Cu matrix and

embedded NbTi superconducting filaments.¹⁵ Averaged-over-direction Young's modulus of copper is 128.7 GPa and that of NbTi is 84.3 GPa. Thus, the stiffness mapping consistently shows the difference of their Young's moduli. Higher stiffness on the edge of the filaments is caused by the effect of the surrounding Cu: The contact area is estimated to be 1–3 μm and includes both materials on the edge. Internal friction of NbTi is higher and very high internal friction appears at some locations, suggesting microcracking or delamination.

In conclusion, we developed a microscopy method for detecting the local internal friction of materials. The critical demand for the isolated oscillator has been accomplished by the noncontacting measurement of the frequency and attenuation by the antenna placed close to the langasite oscillator. We formulated the relationship between the local internal friction and attenuation of the resonator system using a bar-resonance model with the Herizian contact. Because of the simple and isolated oscillator structure, this microscopy will be applied not only to laboratory research but also to a non-destructive test in the field.

This study was supported by an Industrial Technology Research Grant Program in 2004 from the New Energy and Industrial Technology Development Organization (NEDO).

¹C. Zener, *Elasticity and Anelasticity of Metals* (University Chicago Press, Illinois, 1948).

²R. Truell, C. Elbaum, and B. Chick, *Ultrasonic Methods in Solid State Physics* (Academic, New York, 1969).

³A. Nowick and B. Berry, *Anelastic Relaxation in Crystalline Solids* (Academic, New York, 1972).

⁴M. Hirao, H. Ogi, N. Suzuki, and T. Ohtani, *Acta Mater.* **48**, 517 (2000).

⁵H. Ogi, Y. Minami, and M. Hirao, *J. Appl. Phys.* **90**, 438 (2002).

⁶H. Ogi, J. Tian, T. Tada, and M. Hirao, *Appl. Phys. Lett.* **83**, 464 (2003).

⁷J. Tian, H. Ogi, T. Tada, and M. Hirao, *J. Appl. Phys.* **94**, 6472 (2003).

⁸H. Ogi, T. Tada, J. Tian, and M. Hirao, *Jpn. J. Appl. Phys., Part 1* **44**, 4381 (2005).

⁹I. Ohno, *Phys. Chem. Miner.* **17**, 371 (1990).

¹⁰H. Ogi, N. Nakamura, K. Sato, M. Hirao, and S. Uda, *IEEE Trans. Ultrason. Ferroelectr. Freq. Control* **50**, 553 (2003).

¹¹M. Hirao and H. Ogi, *EMATs for Science and Industry: Noncontacting Ultrasonic Measurements* (Springer-Kluwer, Boston, 2003).

¹²G. Yaralioglu, F. Degertekin, K. Crozier, and C. Quate, *J. Appl. Phys.* **87**, 7491 (2000).

¹³M. Tane, T. Ichitsubo, H. Ogi, and M. Hirao, *Scr. Mater.* **48**, 229 (2003).

¹⁴D. Hull and D. J. Bacon, *Introduction to Dislocations* (Pergamon, Oxford, 1984), p. 218.

¹⁵J. Tian, H. Ogi, T. Tada, M. Hirao, and H. Ledbetter, *J. Appl. Phys.* **96**, 133 (2004).